

# MEASURING MOVEMENT AND LOCATION IN ENCLOSED SPACES USING 3-AXIS ANISOTROPIC MAGNETO RESISTIVE SENSOR ARRAY

Alexander J. Weir  
Medical Devices Unit  
Department of Clinical Physics  
NHS Greater Glasgow and Clyde  
Southern General Hospital  
Glasgow, United Kingdom  
email: alexander.weir@nhs.net

Yeong Y. Lee  
School of Medical Sciences  
Universiti Sains Malaysia  
Kota Bahru, Kelantan, Malaysia  
email: justnleey@gmail.com

Kenneth E.L. McColl  
Institute of Cardiovascular  
and Medical Sciences  
University of Glasgow  
Glasgow, United Kingdom  
email: kenneth.mccoll@glasgow.ac.uk

## ABSTRACT

Understanding the physiology of body systems through *in vivo* distance and positional measurement in narrow enclosed spaces presents several major challenges. A technique using a 3-axis anisotropic magneto resistive (AMR) sensor array is reported which has been developed to provide continuous real-time monitoring of the position of the gastro-oesophageal squamo-columnar junction (SCJ) for the study of the pathology of the upper gastrointestinal (GI) tract. A technical review is provided of the AMR sensor array for the measurement of mm distances to provide positional information *in vivo*. The device is used to measure distance along a string of sensors relative to a small magnet that is endoscopically clipped on to the SCJ. The probe consists of an array of 32 sensors mounted on a flexible printed circuit board within a silicone tube and provides a total measurement distance of 217 mm.

## KEY WORDS

Anisotropic magneto-resistive sensor, gastro-oesophageal junction, squamo-columnar junction.

## 1 Introduction

There are many instruments and tools available today for accurately and continuously measuring distance but most rely on physical contact with the material or visual inspection of the location to be measured. When the distance to be measured is not only hidden, but within the human body and in a position that is constantly changing, the methods required for delivery of accurate and stable measurement are considerably more challenging. In recent years monitoring of the structure and function of the gastro-oesophageal junction (GOJ) [1][2][3][4] has provided one example of this challenge.

A variety of investigation tools have been developed to allow monitoring of the structure and function of the GOJ. Most recently, these have involved the clipped attachment of a small magnet at the SCJ [1] and the insertion of probes that lie straddling the GOJ for measuring magnet position, luminal pH, impedance and pressure, where a combination of sensors allows meaningful interpretation

of synchronised data capture, providing the ability to study accurately the luminal environment near to the SCJ (figure 1). The GOJ is known to be highly dynamic and crucial amongst this data is the ability to monitor the location of the SCJ and thus to know when gastric contents have refluxed onto the oesophageal mucosa.

One approach to distance measurement using magnetic positioning in this area was a probe (MKI) consisting of 26 Hall effect sensors mounted as two arrays of 13 sensors on separate flexible printed circuit boards (PCBs) [1], overlapped to provide an effective sensor spacing of 5 mm in two-dimensional space. Although this probe provided valuable results, the principle weakness was orientation in relation to the magnet position. Hall effect sensors were found only to be useful for 2-D position detection when the magnet orientation was optimal such that it directly faced the sensor. In most circumstances it is difficult to predict or control how a magnet clipped at the SCJ would orientate against the sensor during *in vivo* studies. There are many factors that can potentially affect the orientation of the magnet within the gastrointestinal (GI) luminal tract such as the passage of food, folds of the oesophageal wall, contraction of the lower sphincter, heavy secretions, and the presence (shielding effect) of other sensor probes.

To overcome these problems, a further revision of the Hall effect probe (MKII) was developed to sense the magnet position with an effective sensor spacing of 7 mm in three-dimensional space. This was achieved by placing alternate sensors on foldable 'tabs' on the flexible PCB. In this way, the alternate sensors could be positioned orthogonally to their neighbours. Whilst this revision overcame the 2-D limitation of the MKI probe, the overlapping 'tabs' of the flexible PCB design delivered a sensor array that is more rigid than is ideally required for manoeuvring in narrow, winding tracts. This inflexibility was found to place additional mechanical stresses on the sensor pin solder joints leading to an unacceptable mean time before failure.

In this paper we report a new and novel positioning sensor probe based on a 3-axis AMR [5][6] sensor array to allow continuous monitoring of the location of the SCJ in three-dimensional space which resolves the problems expe-

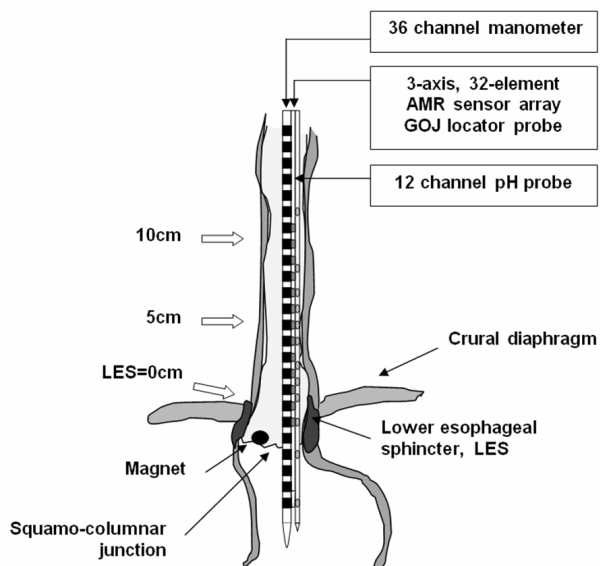


Figure 1: A sketch of the location sensor probe, manometer and pH- catheter within the oesophagus and straddling the GOJ and near to the SCJ

rienced with previous studies and allows the accurate study of the luminal environment close to the SCJ.

## 2 Background

The proliferation of hand held devices such as smart phones with functions supporting applications such as electronic compass, GPS navigation and direction and position sensing has led to the rapid development of accurate, low cost magnetic sensing semiconductor devices. One such device is the Memsic MMC328xMS [7], a 3-axis magnetic sensing system with on-chip signal processing and integrated I<sup>2</sup>C (Inter-Integrated Circuit) bus communications. The functional diagram and the marking illustration (showing the relative x, y, z-plane orientations) of the Memsic MMC328xMS device are shown in figure 2.

These AMR sensors contain special resistors made of a thin permalloy (NiFe magnetic film) on a silicon wafer. An external magnetic field will cause the film to deflect and change its resistance. The resistance change in each axis is measured using a Wheatstone bridge and the corresponding x-plane, y-plane and z-plane deflections are accessible through I<sup>2</sup>C serial communications bus. The I<sup>2</sup>C bus allows the sensor to be directly connected to a micro controller, eliminating the need for A/D converters or timing resources. The AMR sensor is addressable over the I<sup>2</sup>C bus using eight pre-programmed device addresses which correspond to eight part numbers as shown in table 1.

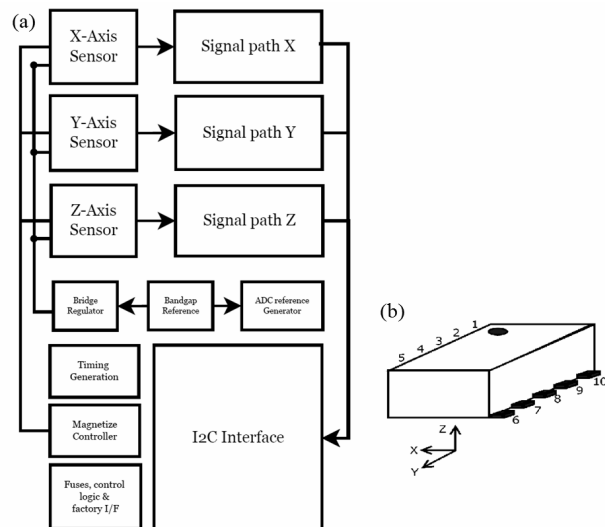


Figure 2: (a) The functional block diagram of the MMC328xMS 3-axis magnetic sensing system, reproduced from [7]; (b) The marking illustration of the MMC328xMS magnetic sensor package, reproduced from [7].

Part number	Package number	7-bit I <sup>2</sup> C Address
MMC3280MS	350	0110000b
MMC3281MS	351	0110001b
MMC3282MS	352	0110010b
MMC3283MS	353	0110011b
MMC3284MS	354	0110100b
MMC3285MS	355	0110101b
MMC3286MS	356	0110110b
MMC3287MS	357	0110111b

Table 1: The MMC328xMS magnetic sensor part numbers and I<sup>2</sup>C addresses, reproduced from [7]

## 3 Method

A sensor array was designed and developed using the AMR sensor. The array consists of 32 sensors mounted at intervals of 7 mm on a single flexible PCB strip. Sensors are arranged in four banks of eight devices, using each of the available internal I<sup>2</sup>C addresses in each bank. The output from each sensor is continually monitored by the micro controller. The sensor values are passed into a software algorithm which sums and interpolates the detected magnetic field strengths, allowing the external magnet location to be determined in relation to the sensor strip.

### 3.1 Equipment Design

#### 3.1.1 MMC328xMS AMR Sensor

The Memsic MMC328xMS AMR sensor is available in a 10-pin ultra-small low profile surface mount LGA package (3 x 3 x 1 mm). This compact physical design was essential for this application in order to minimise the catheter diam-

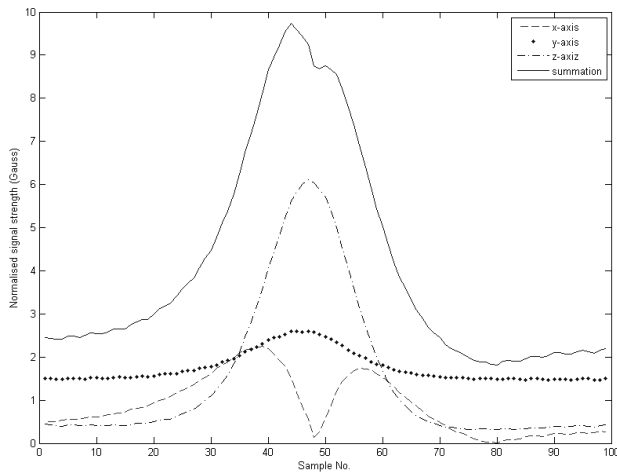


Figure 3: The response of a single MMC328xMS magnetic sensor in the x-plane, y-plane, and z-plane, shown with the xyz summed vector as an ES1547 magnet is moved linearly along the y-axis at a free space gap of 5 mm

eter.

The small magnet clipped at the SCJ creates a magnetic field that causes the sensor to produce a deflection output proportional to the field strength in all 3-axis. Figure 3 shows the response profile for a single sensor as a samarium cobalt medium grade (ES1547) magnet is moved linearly along the y-axis over a range of 7 mm (from the centre of the PCB just below the sensor package to the centre of the PCB just above the sensor package) and a gap of 5 mm, where the gap is the distance in free space between the magnet and the top of the sensor semiconductor package.

The MMC328xMS sensor can measure a magnetic field with a full range of  $\pm 8$  Gauss. However, in the presence of strong external magnetic fields of more than 10 Gauss the permalloy film can distort or flip and upset the sensor characteristics. Fortunately the sensor has been provided with an electrical control capable of resetting the sensor film to a functioning condition if it should inadvertently become distorted.

### 3.1.2 AMR Sensor Array

The 32 sensors are mounted on a flexible PCB strip 4 mm wide and are placed 7 mm apart. The number of sensors and the spacing used for monitoring the GOJ is a compromise between the distance measured, the measuring accuracy required and the system response time and data flow capacity; since all sensors must be interrogated sequentially to determine the position of the magnet. The sensor spacing distance was determined through consideration of the total overall measuring range and the need for adjacent sensors to both detect the magnetic field and allow interpolation between sensors. The system was required to achieve a measuring accuracy of up to 10 mm for effective study of

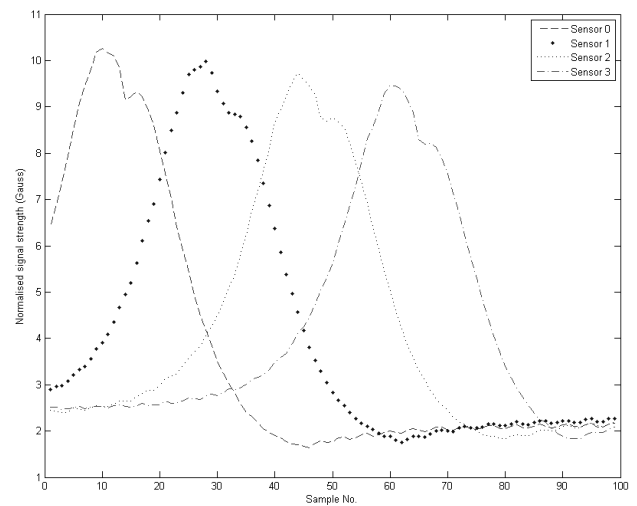


Figure 4: The summed x, y and z-axis magnetic field strengths observed from adjacent MMC328xMS magnetic sensors as an ES1547 magnet is moved linearly along the y-axis at a free space gap of 5 mm.

the GOJ.

The sensors are arranged in four banks of eight such that each sensor may be addressed individually on the I<sup>2</sup>C bus. In this way, the sensor data interface can be multiplexed such that the PCB requires only seven connections to allow for power supplies and communication to all sensors. Figure 4 shows the summed x, y and z-axis magnetic field strengths observed from adjacent MMC328xMS magnetic sensors as a magnet is moved linearly along the y-axis at a gap size of 5 mm. Figure 5 shows a picture of the MMC328xMS magnetic sensor probe in a sheath of silicone tube.

### 3.1.3 Gastro-Oesophageal Junction Locator Instrumentation System

An instrumentation system was designed to support the GOJ location function. It communicates with the AMR sensor and provides a USB interface for data acquisition to a personal computer (PC). A micro controller module within the instrument provides software control for all communication and instrumentation functions.

The instrument provides three interfaces: (i) An LCD display, indicating to the user the sensor nearest the strongest magnetic field, a value proportional to the field strength observed and the interpolated magnet position in mm. (ii) Two DAC outputs, providing analogue signals proportional to sensor signal strength and the interpolated magnet position that provide inputs to a polygraph for synchronisation with pH and impedance probe data. (iii) An isolated USB interface providing a control and data interface to all sensors.

The USB interface is supported by drivers and a Windows PC application which is used to acquire raw data

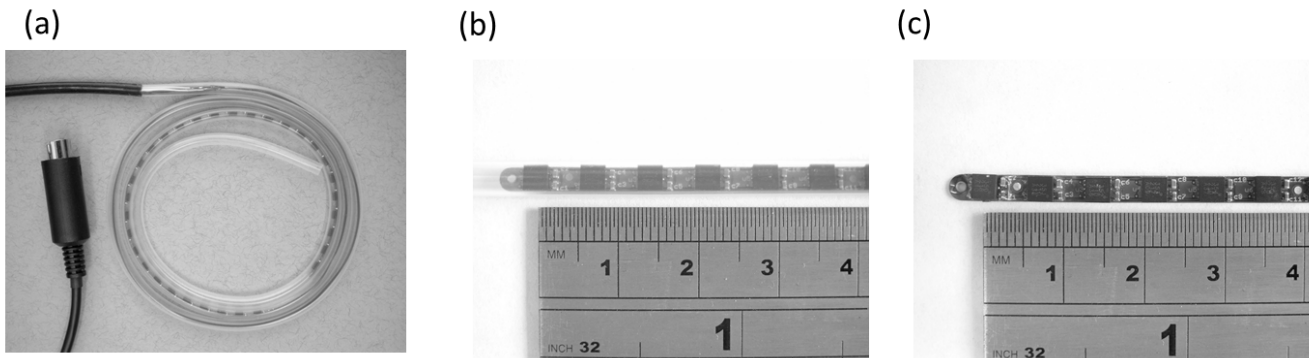


Figure 5: A picture of the MKIII MMC328xMS magnetic sensor probe is shown; (a) coiled with all 32 sensors sheathed in a silicone tube (AlteSil™, Altecweb.com Ltd, UK), (b) with a close-up view of the first six sensors in sensor bank 1 sheathed in silicone, (c) with a clearer view of the first six sensors in sensor bank 1 on a flexible PCB substrate.

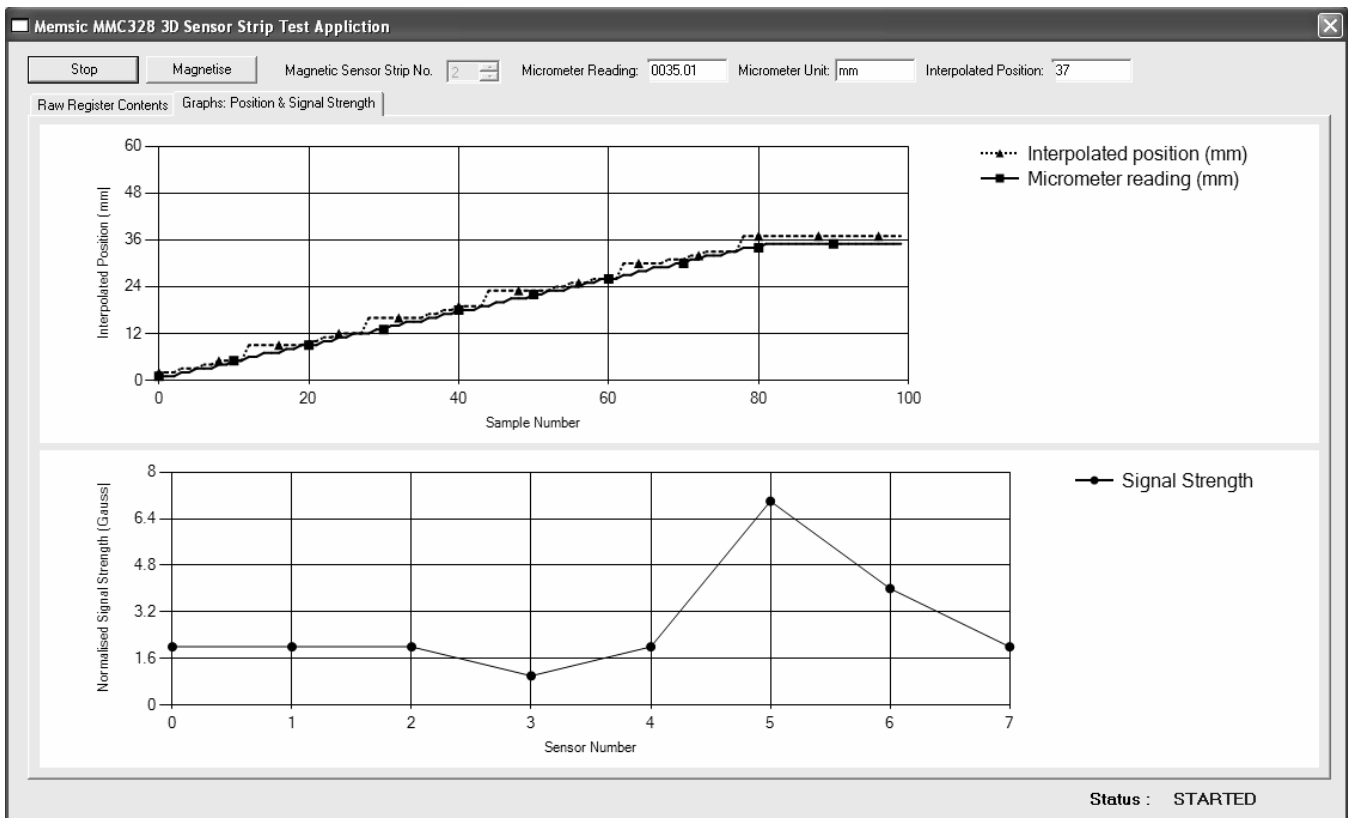


Figure 6: A graphical display of interpolated position and summed signal strength as captured by the sensor strip test application. The upper graph in the application view shows the interpolated sensor reading (mm) and the actual position as measured on a digital micrometer (mm). The lower graph shows the summed signal strength vector (Gauss) for sensors numbered 0 to 7.

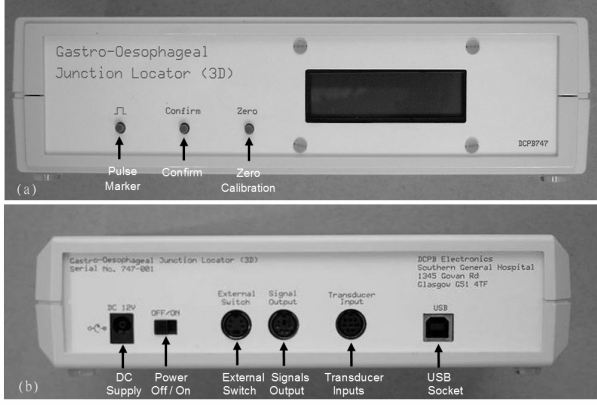


Figure 7: The GOJ locator instrument system front panel (a) with LCD user display and controls and the rear panel (b) with connectivity options.

from each sensor in all three planes and provide graphical views of position and magnetic field strength. Figure 6 shows the graphical display of position and signal strength on the Windows application. On the Windows application view, the upper graph shows the interpolated sensor reading (mm) and the actual position as measured on a digital micrometer (mm), whilst the lower graph shows the summed signal strength vector (Gauss) for up to eight sensors, numbered 0 to 7. Figure 7 shows the GOJ locator instrument system front and rear panel with LCD user output, controls and connectivity options.

The instrument design conforms to EU medical electrical safety standards and is fully isolated from the mains supply.

### 3.1.4 Software

The instrumentation system software architecture is implemented within host and target sub-systems, with communication over a USB 2.0 interface.

The host sub-system consists of software components including an application programmer's interface (API), shared libraries and a USB driver integrated within the Windows operating system running on a PC. A Windows application provides the user with the ability to capture raw data from the AMR sensor probe and continuously monitor the interpolated sensor position and the magnetic field strength detected at each probe sensor. Collectively, these parts realise the application interface.

The target sub-system consists of the embedded software application running on a PIC18F87J50 Microchip micro controller. The target sub-system provides initialisation routines, display and communications functions. The most important function is the interpolation algorithm.

All 32 AMR sensors in the array are sampled in the x, y, z-plane at an interval of 300 ms. For each AMR sensor, the magnitude of the sensor reading in each plane is

summed to provide a single vector  $v_i$ , where

$$v_i = (|B_{i_x}| + |B_{i_y}| + |B_{i_z}|). \quad (1)$$

This vector is then used within an interpolation algorithm. The interpolation algorithm calculates the position  $p(n)$  at sample instance  $n$ . This is done by finding the maximum magnetic signal strength vector  $v_{i_{\max}}$  corresponding to sensor number  $i$ . The sensor offset in mm of  $v_{i_{\max}}$  will correspond to the product of the sensor spacing  $s$  and the sensor number  $i$ . The position  $p$  at sample instance  $n$  is therefore given by

$$p(n) = (s \times i) - \left[ s \times \frac{v_{(i_{\max}+1)}}{v_{i_{\max}} + v_{(i_{\max}+1)}} \right], \quad (2)$$

where

$$v_{(i_{\max}+1)} > v_{(i_{\max}-1)}, \quad (3)$$

and

$$p(n) = (s \times i) + \left[ s \times \frac{v_{(i_{\max}-1)}}{v_{i_{\max}} + v_{(i_{\max}-1)}} \right], \quad (4)$$

where

$$v_{(i_{\max}-1)} > v_{(i_{\max}+1)}. \quad (5)$$

Calculation (2) or (4) will be performed depending on the highest adjacent magnetic signal strength vector  $v_{(i_{\max}+/-1)}$ . This will be at position  $(i-1)$  or  $(i+1)$  depending on the magnet position, as shown in figure 8. In the case where  $v_{(i_{\max}+1)} = v_{(i_{\max}-1)}$ , the position at sample instance  $n$  is simply  $p(n)$  and is given by

$$p(n) = s \times i. \quad (6)$$

### 3.1.5 Magnet

The choice of magnet used in the clipped attachment is of crucial importance to the sensitivity and accuracy of the measurement system. A small number of rare earth disc magnets of different size and type were used during evaluation and testing. These are available in two types; namely neodymium ( $NdFeB$ ) and samarium-cobalt ( $SmCo$ ). These magnets are extremely brittle and are usually covered with a protective coating (e.g. nickel+copper+nickel;  $Ni-Cu-Ni$ ) to prevent them from breaking. Table 2 summarises the magnet specifications used in the testing regime and provides the part numbers.

## 3.2 Testing Protocols

The main feature of the testing regime was the acquisition of sensor readings corresponding to variations in magnet gap, magnet orientation (in the x, y, z-plane) and sensor strip orientation (in the x, y, z-plane) along the full length of the AMR sensor strip. Figure 9 shows a sketch of the AMR system test protocol.

Magnet reference	Size (mm)	Type	Part No.	§Pull (Kg)
Samarium Cobalt Low grade	1 x 1	SmCo10	ES1548	0.015
Samarium Cobalt Medium grade	1 x 1	SmCo16	ES1547	0.026
Samarium Cobalt High grade	1 x 1	SmCo26	EP305SM	0.040
Neodymium N42	1 x 1	Nd2Fe14B	F305-100	0.025
Neodymium N42	2 x 1	Nd2Fe14B	F321-50	0.130

§ Pull force is defined as the maximum mass in kilograms the magnet can lift if acting vertically.

Table 2: A summary of magnet type, size, pull mass and part numbers.

Magnet Reference	Angle (degrees)	Average Error				Maximum Error			
		5mm	10mm	15mm	20mm	5mm	10mm	15mm	20mm
Samarium Cobalt Low grade (ES1548)	0	1.39	2.66	‡n/a	‡n/a	3.61	6.69	‡n/a	‡n/a
	45	0.71	1.48	‡n/a	‡n/a	2.52	4.12	‡n/a	‡n/a
	90	2.66	11.34	‡n/a	‡n/a	5	21.99	‡n/a	‡n/a
	-45	4.72	7.02	‡n/a	‡n/a	7.48	11.3	‡n/a	‡n/a
Samarium Cobalt Medium grade (ES1547)	0	1.97	5.1	‡n/a	‡n/a	4.3	9.2	‡n/a	‡n/a
	45	0.89	1.85	‡n/a	‡n/a	3.32	4.62	‡n/a	‡n/a
	90	2.2	1.58	‡n/a	‡n/a	5.2	5.17	‡n/a	‡n/a
	-45	4.05	8.4	‡n/a	‡n/a	6.67	12.7	‡n/a	‡n/a
Samarium Cobalt High grade (EP305SM)	0	1.02	1.91	3.44	‡n/a	2.43	4.62	8.33	‡n/a
	45	2.76	1.57	1.75	‡n/a	5	4	4.98	‡n/a
	90	2.69	3.87	6.75	‡n/a	4.96	8.17	11.59	‡n/a
	-45	1.49	4.67	5.71	‡n/a	4.11	7.84	10.02	‡n/a
Neodymium N42 1 x 1 (F305-100)	0	0.66	1.31	2.36	‡n/a	2.1	6.52	7.4	‡n/a
	45	0.96	1.88	2.92	‡n/a	3.49	5.28	7.07	‡n/a
	90	2.03	3.82	3.99	‡n/a	4.14	7.97	8.82	‡n/a
	-45	2.43	3.75	8.97	‡n/a	4.91	7.24	17.02	‡n/a
Neodymium N42 2 x 1 (F321-50)	0	3.38	2.55	2.87	3.19	6.93	5.82	7.59	6.83
	45	2.49	3.95	1.37	1.84	9.16	7.67	3.37	4.83
	90	2.37	2.97	5.91	6.88	7.16	5.9	9.79	11.33
	-45	2.75	1.14	1.95	6.55	6.42	2.46	5.54	14.05

‡ At some gap distances, the detected field strength of the reference magnet is too small to provide a signal that is distinguishable from the Earth's background magnetic field strength (0.25 to 0.65 Gauss) and a distance or position measurement cannot be interpolated.

Table 3: A comparison of magnet performance and interpolation error for different gap distance and orientation.

The barrel length of each magnet was 1 mm and barrel diameter varied between 1 (for the ES1548, ES1547, EP305SM and F305-100) and 2 mm (for the F321-50). For each test, the magnet was orientated at an angle of 0, +45, -45 or 90 degrees relative to the upper face of the sensor component and then traversed across the AMR sensor strip at a selected test gap of 5, 10, 15, or 20 mm. As the magnet traversed across the AMR sensor strip the software application automatically recorded the actual position of the magnet from a digital micrometer and the interpolated position from the GOJ locator instrumentation system.

During the early stages of testing, a major concern was prevention of sensor saturation. Typically, this occurs when the test magnet lies within approximately 2 to 3 mm of the sensor and there is a danger that the magnetic field strength detected may rise above +/- 10 Gauss. Removal of the field and resetting the sensor always returned the sensor to a functioning condition when this condition was detected.

## 4 Results

Using the test protocol described in figure 7, the performance of each of the magnets listed in table 2 was observed in terms of the average interpolation error and maximum interpolation error when compared to a digital micrometer reading of the actual magnet position relative to the AMR sensor strip at gaps of 5, 10, 15 and 20 mm. Table 3 provides a summary of the results.

For all magnets tested, the effect of changing the magnet orientation between 0 and 90 degrees was observed to alter the average and maximum interpolation errors observed, and the results were not consistent as the magnet range increased. This can be explained by considering the magnetic field shape or profile. The alignment of this profile with the sensor has an important bearing on the accuracy of the interpolated position. At close range the higher field strength magnets can saturate the device, as shown by the neodymium N42 2x1 (F321-50) magnet at gap of less than 5 mm, whilst variations in field profile show marked

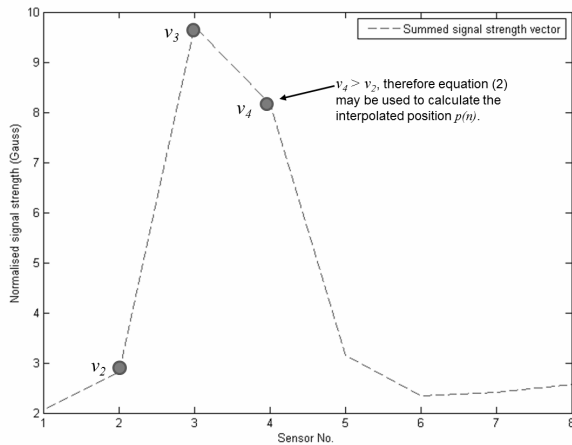


Figure 8: A graphical display of the interpolated position calculation, showing the summed signal strength vector for eight sensors in a single bank. The highest signal strength is detected at  $v_3$  and the next highest adjacent signal strength is at  $v_4$ . In this case, equation (2) may be used to determine the interpolated position.

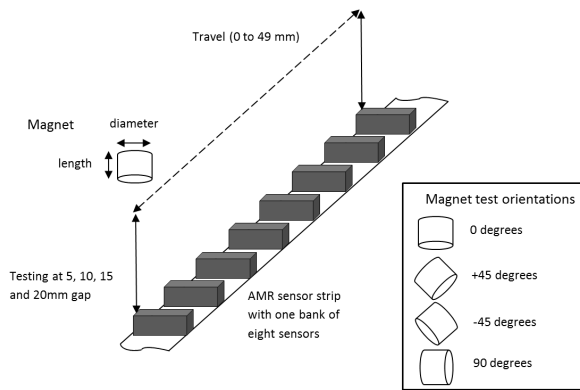


Figure 9: A sketch of the AMR system test protocol. A magnet of length 1 mm and diameter 1-2 mm is traversed across the AMR sensor strip at a selected test gap of 5, 10, 15, or 20 mm. The magnet for each test was orientated at an angle of 0, +45, -45 or 90 degrees relative to the upper face of the sensor component.

differences in accuracy in the samarium cobalt medium grade (EP305SM) and neodymium N42 1x1 (F305-100) magnets. With the weaker field strength magnets, the observed interpolation accuracies achieved are less than 1 mm at a gap of 5 mm when the magnet orientation tends to around +45 degrees. However, this accuracy drops off quickly when the orientation reaches around -45 degrees.

Although the low grade ES1548 and medium grade ES1547 samarium cobalt magnets performed reasonably well at a gap of 5 mm and below, the field strength of these magnets drops off very quickly above 5 mm, whilst at around 10 mm gap distance the observed maximum error instance can be well over 10 mm. This limits the usefulness of the low grade and medium grade samarium cobalt magnets to only short distances, at an effective gap of 5 mm or less.

In the bench tests, the samarium cobalt high grade (EP305SM) magnet consistently achieved very good results at a gap distance of 5 mm, where the average interpolation error is less than 3 mm, and at a gap distance of 10 mm, where the average interpolation error is less than 5 mm. However, above a gap distance of 10 mm, although the performance is much better than the weaker field strength magnets, the maximum error can drift above 10 mm. In comparison with the neodymium N42 1x1 (F305-100), the EP305SM performance above 10 mm is marginally better, however the F305-100 achieves a better accuracy at close range.

Finally, the neodymium N42 2x1 (F321-50) is shown to be less accurate than the EP305SM and F305-100 magnets at gap distances of less than 10 mm, however it achieves much more accurate interpolation results than the other magnets tested at gap distances above 10 mm, even achieving an average interpolation error below 7 mm at a gap distance of 20 mm from the sensor array. The non-linear average error observed below 5 mm is most probably due to saturation within the magnetic sensor and the much wider magnetic field profile produced as a result of doubling the barrel diameter.

In summary, the interpolation error is minimal when the magnetic field is perpendicular to the x, y or z-planes of the AMR sensor and the gap distance between the sensor and the magnet is sufficiently large to prevent saturation but sufficiently small to allow the magnet field strength to be detected relative to other magnetic noise sources, such as the Earth's background magnetic field. Furthermore, the maximum effective gap distance may be significantly reduced by the shielding effect of additional sensor probes etc. Interestingly, in comparison to the Hall effect devices used in the MKI and MKII sensor probes, the AMR magnetic sensor probe was observed to be at least twice as sensitive to the F321-50 magnet at distances of up to 20 mm.

## 5 Discussion

The test results have confirmed that the 3-axis AMR sensor array positional measurement system described by this

paper can achieve a target interpolation accuracy of 10 mm or much less for all devices at a gap distance of up to 5 mm. However, when the sensor target magnet is a neodymium N42 2x1 (F321-50) the system can achieve an average error of less than 7 mm with a gap size of up to 20 mm.

In the case of *in vivo* measurements such as the gastro-oesophageal SCJ however, it is necessary to consider the additional practicalities of distance measurement. As described in this paper, these include allowances for the wall thickness of the catheter silicone sheath, the shielding effect caused by the inclusion of additional sensor probes such as for pH and pressure sensing, and biological features such as the uneven walls of the oesophagus mucosa and the mucus coating effect. The optimal reference magnet in the comparison study presented, given consideration for an adequate gap size to allow for a minimum distance between the magnet and sensor, is the neodymium N42 2x1 (F321-50).

## 6 Conclusion

The combination of the neodymium N42 2x1 magnet, the 32 element AMR sensor array and instrument system with the supporting interpolation algorithm described by this paper, provides an extremely useful device for the *in vivo* position measurement system for study of the dynamic behaviour of the GOJ.

The migration from previous Hall effect sensor probes to AMR sensor probes for *in vivo* positional measurement of this type provides a significant step forward. The smaller foot print of the AMR sensors and the improved sensing performance in three axis provides a more flexible, durable and accurate solution. Indeed, new and improved versions of the MMC328xMS have been released since this study began [8] [9]. The newer devices offer potential improvements in performance in comparison to the current system, but perhaps the most attractive aspect of the new sensors is the more compact package size (2 x 2 x 1 mm). These smaller sensor package sizes may be used to develop a catheter with a diameter reduction of between 1 and 2 mm, providing a more flexible and more comfortable solution for future studies.

## References

- [1] Y.Y. Lee, J.P. Seenan, J.G. Whiting, E.V. Robertson, M.H. Derakhshan, A.A. Wirz, D. Smith, C. Hardy, A. Kelman, P. Connolly, K.E. McColl. Development and validation of a probe allowing accurate and continuous monitoring of location of squamo-columnar junction. *Med Eng Phys*, 34, 279-89, 2012.
- [2] Y.Y. Lee, J.G. Whiting, E.V. Robertson, M.H. Derakhshan, D. Smith, K.E. McColl. Measuring movement and location of the gastroesophageal junction: research and clinical implications. *Scand J of Gastroenterol*, 48, 401-11, 2013.
- [3] Y.Y. Lee, J.G. Whiting, E.V. Robertson, M.H. Derakhshan, A.A. Wirz, D. Smith, D. Morrison, A. Kelman, P. Connolly, K.E. McColl. Kinetics of transient hiatus hernia during transient lower esophageal sphincter relaxations and swallows in healthy subjects. *Neurogastroenterol Motil*, 24, 990-e539, 2012.
- [4] J.G. Whiting, N. Djennati, Y.Y. Lee, E.V. Robertson, M.H. Derakhshan, P. Connolly, K.E. McColl. Towards minimally invasive monitoring for gastroenterology - An external squamocolumnar junction locator. *Conf Proc IEEE Eng Med Biol Soc 2012*, 1575-7, 2012.
- [5] T.R. MacGuire, R.I. Potter. Anisotropic magnetoresistance in ferromagnetic 3d alloys. *Magnetics, IEEE Transactions on*, vol.11, no.4, pp.1018-1038, 1975.
- [6] I. Genish, Y. Kats, L. Klein, J.W. Reiner, M.R. Beasley. Paramagnetic anisotropic magnetoresistance in thin films of SrRuO<sub>3</sub>. *Journal of Applied Physics*, vol.95, no.11, pp.6681-6683, 2004.
- [7] MEMSIC MMC328xMX Rev. C Datasheet, (c)MEMSIC, Inc., One Technology Drive, Suite 325, Andover, MA01810, USA, March, 2011.
- [8] MEMSIC MMC328xMA Rev. D Datasheet, (c)MEMSIC, Inc., One Technology Drive, Suite 325, Andover, MA01810, USA, May, 2012.
- [9] MEMSIC MMC3316xMT Rev. A Datasheet, (c)MEMSIC, Inc., One Technology Drive, Suite 325, Andover, MA01810, USA, October, 2012.